Strong coupling of topological edge states enabling group-dispersionless slow light in magneto-optical photonic crystals

Jianfeng Chen,* Wenyao Liang,* and Zhi-Yuan Li†
School of Physics and Optoelectronics, South China University of Technology, Guangzhou 510641, China

(Received 17 July 2018; published 8 January 2019)

We investigate a two-way waveguide constructed by bringing close two identical magneto-optical photonic crystals which each supports a counterpropagating topological one-way edge state. We find a unique slow-light state that exhibits a very small group velocity ($n_g = 529.2$), a zero group-velocity dispersion, distortionless pulse transport, and ease to be magnetically tuned within a broad frequency range, simultaneously. We show that this unique group-dispersionless slow-light state originates from the strong coupling of the two counterpropagating topological states, which causes complete exchange and transfer of energy flow between them, induces a vortexlike close loop of energy transport channel around the source, leads to complete destructive interference in the far field, and finally results in a very slow propagation velocity of electromagnetic waves. These results indicate that deeply digging into the interaction between photonic topological states can help to open up an arena in topological physics and find great potential of applications such as optical buffer memories and enhanced light-matter interaction.

DOI: 10.1103/PhysRevB.99.014103

I. INTRODUCTION

Topological insulators are new states of quantum matter, whose bulky states are prohibited while surface states are conductive and topologically protected within the energy spectrum of band gap [1]. Many studies have shown that topological states show essentially single-particle behavior of electrons and one can establish an analogy relationship with photon behaviors called photonic topological states [2–7], which are robust against scattering from disorder and immune to backscattering [8–16]. Photonic topological states have been found and confirmed in different structures and have inspired a number of novel phenomena, such as unidirectional guided waves [17–20], *Z*-sharp-bend waveguides [21–25], spin-dependent transportation [26–32], valley states [33–37], Weyl points [38–40], and nodal chains [41].

A prominent way to create photonic topological states is magneto-optical photonic crystal (MOPC) immersed into an external dc magnetic field [42–46]. The properties of topological edge states can be characterized by the Chern number C [47,48]. The gap Chern number ($C_{\text{gap}} = \sum C_i$) can be calculated by summing the Chern numbers of all the bands below the band gap. For a line-defect waveguide, the number of one-way edge states is determined by ΔC_{gap} of two composite structures, and the sign of ΔC_{gap} determines the transport directions of the edge states [47–50].

Up to now, most research about photonic topological states in MOPCs utilize gapped materials [such as metal plate or dielectric photonic crystal (PC)] with $C = 0$ as a confinement barrier to accompany a MOPC with a nonzero Chern number to construct a one-way waveguide [49–52]. In contrast, the studies about the waveguide composed of two MOPCs with the same Chern numbers are very scarce perhaps due to the assumption that little novel physics can be expected in this topologically trivial photonic system. Yet we will show in this paper that such a waveguide can provide a mechanism to create a unique group-dispersionless slow-light state due to the strong interaction between the two counterpropagating topological one-way edge states supported in the two composite semi-infinite MOPCs.

II. BAND STRUCTURAL ANALYSIS OF SLOW LIGHT MODES

We first consider two isolated one-way edge states in two separated square-lattice MOPC in Figs. 1(a) and 1(b). A metallic cladding (marked red color) is used near the edge of each MOPC to form a waveguide whose width is $w_d = 0.5a$ with $a = 3.87$ cm being the lattice constant. Applying a dc magnetic field in the out-of-plane ($+z$) direction will induce strong gyromagnetic anisotropy in yttrium-ion-garnet, and the permeability becomes a tensor as follows [42–44]:

$$\hat{\mu} = \begin{pmatrix} \mu_r & j\mu_k & 0 \\ -j\mu_k & \mu_r & 0 \\ 0 & 0 & 1 \end{pmatrix}, \tag{1}$$

where $\mu_r = 1 + \omega_m(\omega_0 + j\alpha\omega)/[(\omega_0 + j\alpha\omega)^2 - \omega^2]$, $\mu_k = \omega\omega_m[(\omega_0 + j\alpha\omega)^2 - \omega^2]$, with $\omega_0 = 2\pi\gamma H_0$ being the resonance frequency, $\gamma = 2.8$ MHz/Oe being the gyromagnetic ratio, $\omega_m = 2\pi\gamma M_0$ being the characteristic circular frequency, with M_0 being the saturation magnetization. $\alpha = 0$ is the damping coefficient.

In Figs. 1(a) and 1(b), the source locates in the center of each waveguide, and two isolated one-way edge states propagating leftward and rightward are excited at the edges of the

*These authors contributed equally to this work.
†phzyli@scut.edu.cn

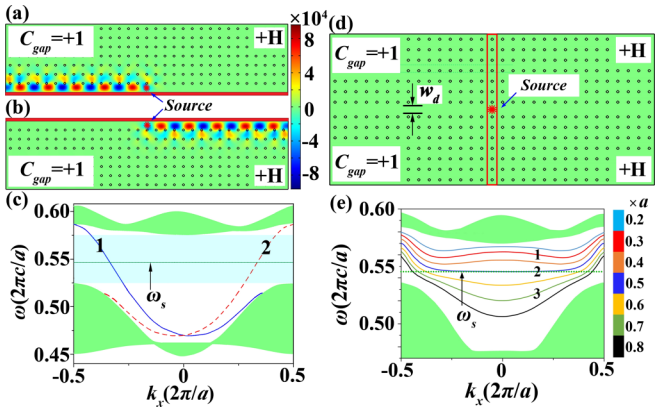

FIG. 1. (a), (b) E_z fields for two one-way edge states (LES and RES). (c) Band structures for the edge states in (a) and (b). (d) Line-defect waveguide constructed by two same MOPCs with the same $C_{\text{gap}} = +1$. A supercell is marked by the red frame. (e) Coupling-band structures of different waveguide widths.

two separated MOPCs at $\omega_s = 0.5454$ [in units of $(2\pi c/a)$, with c being the light speed in vacuum]. The band structures for the two one-way waveguides are calculated and shown in Fig. 1(c) together when $H_0 = 1600$ G. Apparently, there exist two different one-way edge states (symmetric bands 1 and 2) in the photonic band gap, which correspond to the leftward and rightward one-way edge states (called LES and RES) in waveguides (a) and (b), respectively. Therefore, two isolated one-way edge states propagating in opposite directions do coexist in the MOPC waveguides.

How about bringing together two opposite one-way topological states? To find the answer, we construct a waveguide by moving two MOPCs in Figs. 1(a) and 1(b) close to each other head by head, as shown in Fig. 1(d). It should be emphasized that keeping a line defect ($w_d \neq 0$) in the system is very important for the observation of the exotic strong countercoupling behavior. There is no metallic cladding here and ΔC_{gap} is zero for this waveguide. This implies that this waveguide is no longer a one-way waveguide; instead, it supports two symmetric counterpropagating topological one-way edge states with mutual coupling between them. Some unexpected exotic properties can arise due to the strong interaction between these counterpropagating one-way topological edge states.

Figure 1(e) shows the coupling-band structures for different w_d ranging from $0.2a$ to $0.8a$ by using the finite-element method. In the middle part of the Brillouin zone $-0.3 < k_x < 0.3$, for broad waveguides with $w_d = 0.6a$, $0.7a$, and $0.8a$, their bands are convex in profile, while for narrow waveguides with $w_d = 0.2a$, $0.3a$, and $0.4a$, their bands have concave profiles. Right at $w_d = 0.5a$, the band exhibits a flat profile. Moreover, as w_d decreases, the coupling-band is attracted gradually from the lower band to the upper band of the photonic band gap. This physics should be deeply understood upon the interaction picture between two counterpropagating one-way edge states. In a waveguide, there should always be coupling between these states because their electromagnetic (EM) field profiles overlap mutually in space, but the strength closely depends on the wave-vector difference $\Delta k_x = k_{x+} - k_{x-}$ (determining the phase matching or mismatching) as well as w_d (determining the distance and the spatial overlap degree between the two states). Generally, the smaller $\Delta k_x = k_{x+} - k_{x-}$, the stronger the coupling strength is, leading to greater attraction strength of the middle part than those near both edges of the Brillouin zone. Especially, the flatband can be considered as the critical point where the transition from the concave band to the convex band (the so-called band inversion) occurs. The unique flatband dispersion profile may produce a peculiar slow-light state with large group index and zero group dispersion simultaneously. It should be noticed that the slow-light state is not a topologically protected one-way state. However, the physical mechanism of such a slow-light state is attributed to the strong coupling of two counterpropagating topological edge states, which is totally different from conventional dielectric PC waveguides with slow light at the Brillouin zone edge but with large group-velocity dispersion (GVD). What is more, the slow-light state studied here possesses merits of very small group velocity, zero group-velocity dispersion, distortionless pulse transport, and ease to be magnetically tuned within a broad frequency range simultaneously, which will be studied in detail in the following discussions.

III. PHYSICAL MECHANISM OF SLOW LIGHT BASED ON COUPLING OF TOPOLOGICAL STATES

We choose three bands of $0.3a$, $0.5a$, and $0.7a$ (i.e., bands 1, 2, and 3) and $\omega_s = 0.5454$ to study the influence of w_d on the countercoupling effect. This typical frequency is denoted by the green dotted line in Fig. 1(e). We examine the transport behavior of these waveguides by setting a point source at the center of the waveguide and looking into the radiation-field profile. Figure 2(a1) shows that the E_z field is two way and dominantly composed of LES and RES for $w_d = 0.7a$. For the right side of the source, the E_z field can be divided into two parts. The first part is the right forward-propagating wave **d** which is down-shifted and concentrated at the edge of the lower MOPC (recognized as RES). The other part, the backward-propagating wave **d′** which is up-shifted and concentrated at the edge of the upper MOPC (recognized as LES). Figure 2(a2) shows that most of the energy flow propagating rightward is concentrated along the edge of the lower MOPC and evolves into RES, while a small amount is coupled to counterpropagate along the edge of the upper MOPC and evolves into LES. This phenomenon originates from the countercoupling effect of one-way edge state of the upper MOPC. In this case, the upper MOPC not only confines the E_z field in the waveguide but also couples part of the E_z field to propagate backward. For the left side of the source, the field and energy flux transport is antisymmetric with the right side of the source.

When w_d is reduced to $0.5a$, the flatband 2 denoted in Fig. 1(e) is formed, implying that a slow-light state can be excited. In Fig. 2(b1), the E_z field is mainly concentrated around the source and decays quickly away from the source. A close look shows that the field profiles are still composed of oppositely propagating RES (part **d**) and LES (part **d′**) on the right side, and LES (part **u**) and RES (part **u′**) on the left side, but now the strengths of **d** and **d′**, as well as **u** and **u′**,

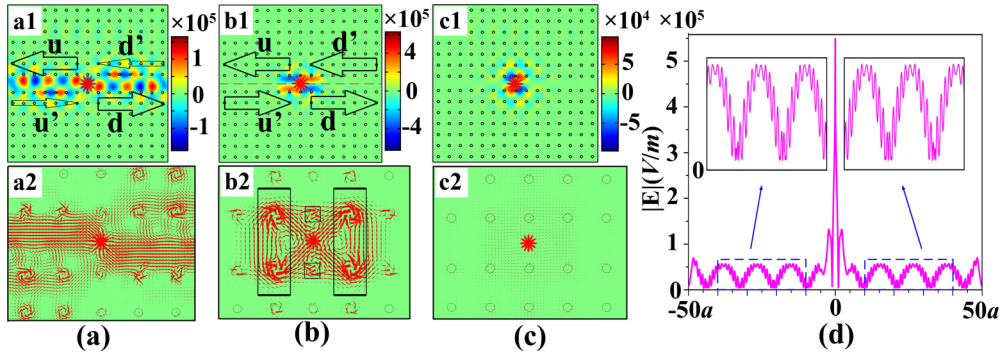

FIG. 2. (a1), (a2), and (a3) are E_z field distributions, while (a2), (b2), and (c2) are Poynting vector distributions for waveguides with $w_d = 0.7a$, $0.5a$, and $0.3a$. The size and direction of the black arrow characterize the strength and propagation direction of EM wave, respectively. (d) Amplitude of electric field along the dashed line at the center of the waveguide with a length of $100a$ in (b1).

are nearly equal to each other. Additionally, in Fig. 2(b2), in the vertical direction, the energy flow fleetly evanesces due to the band gap, while in the horizontal direction, the energy flow around the rods marked by squares is much weaker than those around the four rods marked by rectangles. Obviously, the energy flow gathering mainly around the source flows counterclockwise and forms a close loop. This is because the strong coupling effect leads to the complete exchange and transfer of energy flow between the forward- and backward-propagating EM waves. In Fig. 2(d), the field intensity decays drastically away from the source and eventually propagates stably with regular fluctuation amplitude in the far-field region, forming a standing-wavelike state, which can be regarded as the superposition (destructive interference) of primary forward and secondary backward-propagating edge states. When w_d further reduces to $0.3a$, ω_s drops into the band gap and the E_z field is completely evanescent within the MOPCs. In conclusion, the mutual coupling between the one-way topological RES and LES and the dispersion profile of the consequent coupling band as sensitively affected by w_d will provide a physical mechanism for generating a peculiar slow-light state as discussed previously.

Figure 3 shows another way to deeply explore the physics behind the unique flatband. We choose five points $M_1(0.5454)$, $M_{2\pm}(0.5475)$, and $M_{3\pm}(0.5645)$ to calculate their eigenmode-field profiles, as shown in Fig. 3(b). For $M_1(0.5454)$, the lowest point of the flatband, RES and LES are degenerate at $k_x = 0$. They couple and interfere destructively mutually to create a slow-light state whose group velocity is nearly zero. The eigenmode-field profile depicted in Fig. 3(b) for M_1 mode is nearly antisymmetric (an odd mode), confirming that the origin of this mode is the destructive superposition of degenerate RES and LES, where the field is close to $E_{M_1} = E_{RES} - E_{LES}$. This eigenmode analysis is perfectl1y consistent with the wave and flux analysis made in Figs. 2(b1), 2(b2), and 2(d), further confirming the appearance of the slow-light state. As the frequency increases to $M_{2\pm}(0.5475)$ and $M_{3\pm}(0.5645)$, the strength of countercoupling effect becomes less and less. The consequent coupling mode is no longer the superposition of RES and LES with equal but opposite coefficient, instead, it reads $E_M = c_R E_{RES} + c_L E_{LES}$, where the superposition coefficient c_R is quite different from c_L in strength, indicating that the modal transformation and energy conversion from RES to LES and vice versa from LES to RES are far from complete under this nondegenerate coupling condition, leading to degrading of the slow-light state originated from the destructive interference between RES and LES. Therefore, for waveguide modes $M_{3\pm}(0.5645)$, the modal-field profile looks more like an even mode, and at the same time the radiation wave can depart from the light source by a significantly increased speed. This eigenmode picture accords well with the wave transport analysis made in Fig. 2.

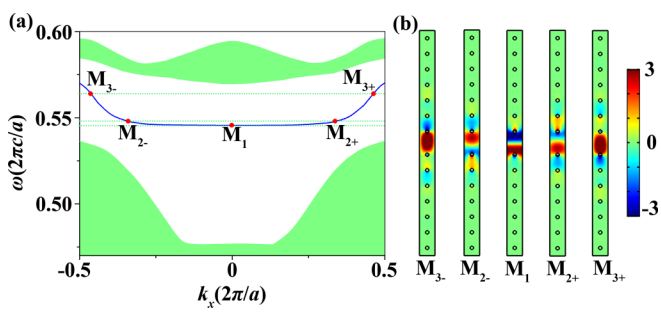

FIG. 3. (a) Flatband structure with $w_d = 0.5a$. (b) Eigenmode fields for different points marked in Fig. 3(a).

IV. BROADBAND MAGNETIC TUNABILITY OF SLOW LIGHT

A unique property of the slow-light states enabled by the strong countercoupling between topological RES and LES in MOPCs is the ease of tunability. Compared with conventional dielectric (silicon, silicon carbide, and others) PCs [53–55], the dispersion relationship of EM wave transport in MOPCs can be easily modulated by adjusting the external magnetic field H_0. In Fig. 4(a), as H_0 increases gradually from 1000 to 1900 G, the slow-light flatband is attracted gradually up from 0.465 to 0.567 in the middle part of the Brillouin zone within the band gap, and the tunability is very prominent. Through this apparent modulation effect, many applications can be achieved, such as continuously tunable group velocity at a single frequency and tunable slow light within a broad frequency range, which is very beneficial to solve the contradiction between slow light and narrow bandwidth.

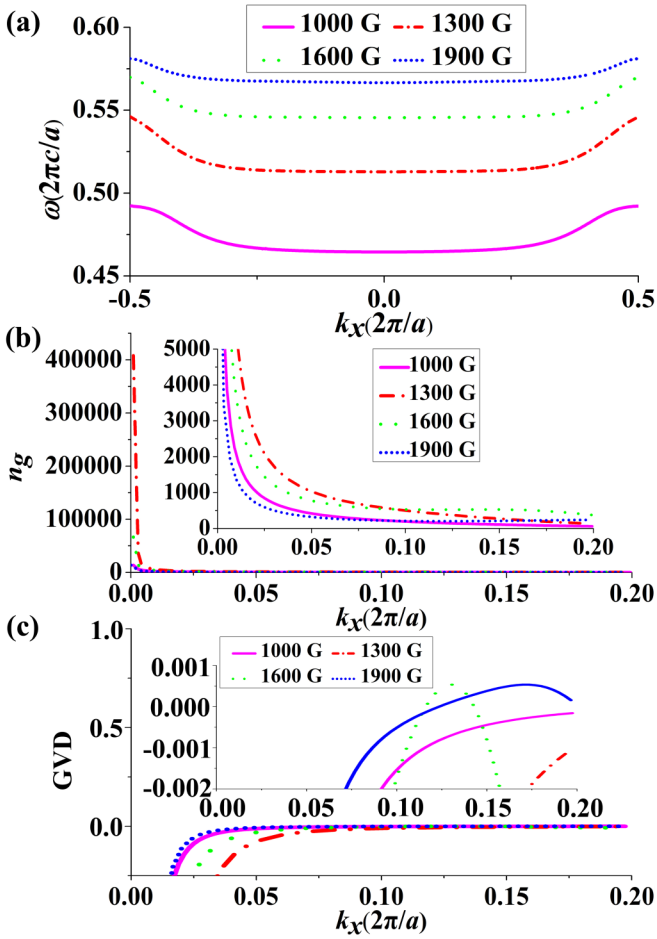

FIG. 4. (a) Flatbands for different H_0. (b) Group index of the waveguide. (c) GVD of the EM wave. The coordinates have nested the partial enlargements diagram in detail.

Several parameters, the group velocity ($v_g = d\omega/dk_x$), the group index ($n_g = c/v_g$), and the GVD [GVD $= d(1/v_g)/d\omega = d^2k_x/d\omega^2$] are used for characterizing the slow-light state. We mainly focus on how slow v_g is and how low GVD can reach in the MOPC system. Since ω increases monotonously with increasing k_x, we use k_x instead of ω to plot $n_g - k_x$ and GVD $- k_x$, and the results are shown in Figs. 4(b) and 4(c). In Fig. 4(b), when k_x gradually increases, n_g falls down rapidly. Specifically, at $k_x = 0$, when $H_0 = 1300$ G, n_g reaches the maximum of 407 899, and when $H_0 = 1000$ G, n_g reaches the minimum of 13 682. In Fig. 4(c), the magnitude of GVD descends sharply as k_x grows from zero, when $H_0 = 1600$ G, GVD $= 0$ appears at $k_x = 0.115$ and 0.143, and their corresponding group indices are $n_g = 523.7$ and 529.2, respectively. Besides, when $H_0 = 1900$ G, GVD reaches zero at $k_x = 0.121$ and 0.195, and their corresponding n_g are 202.4 and 238.5, respectively. Hence, by utilizing the strong coupling of counterpropagating one-way topological edge states, the propagation of light can reach a group-dispersionless slow-light state, where both the group velocity and GVD can reach very low values simultaneously.

We look closely at the local dispersion profile around the group-dispersionless slow-light state, as displayed in

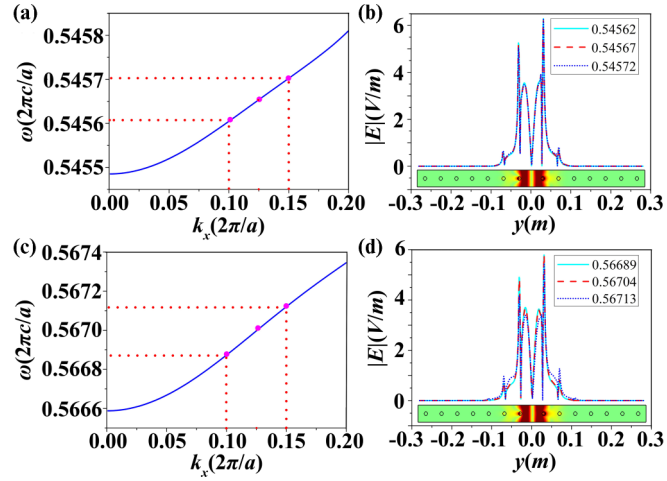

FIG. 5. (a), (c): Local dispersion bands for $H_0 = 1600$ and 1900 G, respectively. (b), (d): Eigenmodes of $|E|$ along y direction at different frequencies denoted by the three magenta points in (a) and (b).

Figs. 5(a) and 5(c) in the ranges marked by dotted lines, i.e., $0.10 < k_x < 0.15$. In this region, the dispersion profile is close to a perfect straight line with a very gentle slope, which means the group velocity is very small, and more importantly the GVD is near zero or exactly zero simultaneously. These results are in good accordance with the calculation results shown in Fig. 5(c). Moreover, we examine the eigenmode-field profiles of the slow-light states within the frequency ranges. The modal profiles for three frequencies corresponding to the lower edge, the middle, and the upper edge of the wave vector range ($0.10 < k_x < 0.15$) are calculated and displayed in Figs. 5(b) and 5(d). When $H_0 = 1600$ G, the eigenmode-field intensity maps corresponding to three frequencies are nearly perfectly overlapping, which indicate that all the modes within the dispersionless slow-light frequency region in Fig. 5(a) have the identical field profile. As for $H_0 = 1900$ G, the intensity map of 0.567 13 is slightly offset from the maps of the other two frequencies, as seen in Fig. 5(d). Obviously, this difference in the eigenmode-field intensity maps originates from the GVD. Integrating all the information of dispersion profile, group velocity, GVD, as well as the modal-field profile, we can assure that EM wave can propagate under the group-dispersionless slow-light state, so an EM pulse can maintain distortion-free propagation along the MOPC waveguide in a very slow speed that is 2–3 orders of magnitude smaller than light speed in vacuum. This qualitative analysis can be placed into a more mathematical way, where the electric field of the pulse transporting in the waveguide can be expressed as the superposition of all the composite monochromatic waveguide modes (note not plane waves) as

$$E(\mathbf{r}, x, t) = \int dk_x E(\mathbf{r}, k_x) A(k_x) \exp[ik_x x - i\omega(k)t]$$
$$= E(\mathbf{r}) \exp[i(k_0 x - \omega_0 t)] \int dk_x A(k_x)$$
$$\times \exp[i(v_g t - x)(k_x - k_0)]. \quad (2)$$

Here $A(k_x)$ is the wave-packet envelope function (e.g., a Gaussian function) of the pulse. In reaching the final step of Eq. (2), we have taken into account the near-zero dispersion in both the modal-field profile [$E(\mathbf{r}, k_x) = E(\mathbf{r})$, with $\mathbf{r}$ being the transverse space site] and group velocity [$v_g(k_x) = v_g$] within the frequency window in Fig. 5, so that $\omega(k_x) = \omega_0 + v_g(k_x - k_0)$. Obviously, a slow-light (in v_g) distortionless pulse propagation behavior is reached at the group-dispersionless slow-light state. Both the modal profile and dispersion profile of the waveguide mode make equally critical contribution to this unique feature rarely encountered in micro/nanoscale optical devices.

V. CONCLUSIONS

In summary, we have deliberately constructed a two-way waveguide by bringing close to each other two identical MOPCs which each supports a counterpropagating one-way topological edge state. However, we have discovered a group-dispersionless slow-light state in this two-way waveguide existing near the Γ point of a flatband, which exhibits a very small group velocity (or a very large group index about 529.2), a near-zero GVD, and nearly identical modal-field profile within a finite frequency window simultaneously. Moreover, this slow-light state can be magnetically tuned within a broad frequency range. As a result, a pulse can propagate very slowly and without distortion along the MOPC waveguide. This discovery may offer useful hints to explore deeply various interaction effects between photonic topological states. The unique group-dispersionless and broadband tunable slow-light state may have great potential in many application fields, such as optical buffer memories, optical switches, and especially in enhanced light-matter interaction. More importantly, our work may open up a frontier of topological physics where fruitful physical phenomena and useful functionalities can be found and achieved by deeply exploiting various interaction effects between photonic topological states.

ACKNOWLEDGMENTS

The authors are grateful for the financial support from the National Natural Science Foundation of China (Grants No. 11504114 and No. 11434017), Science and Technology Program of Guangzhou, Guangdong Innovative and Entrepreneurial Research Team Program (Grant No. 2016ZT06C594), National Key R&D Program of China (Grant No. 2018YFA 0306200), and the Fundamental Research Funds for the Central Universities (Grants No. 2015ZZ056 and No. 2017BQ040).

[1] M. Z. Hasan and C. L. Kane, Rev. Mod. Phys. **82**, 3045 (2010).
[2] S. Raghu and F. D. M. Haldane, Phys. Rev. A **78**, 033834 (2008).
[3] F. D. M. Haldane and S. Raghu, Phys. Rev. Lett. **100**, 013904 (2008).
[4] A. B. Khanikaev, S. H. Mousavi, W.-K. Tse, M. Kargarian, A. H. Macdonald, and G. Shvets, Nat. Mater. **12**, 233 (2013).
[5] L. Lu, J. D. Joannopoulos, and M. Soljačić, Nat. Photonics **8**, 821 (2014).
[6] A. B. Khanikaev and G. Shvets, Nat. Photonics **11**, 763 (2017).
[7] X. Y. Xie, H. F. Wang, X. Y. Zhu, M. H. Lu, Z. D. Wang, and Y. F. Chen, Opt. Express **26**, 24531 (2018).
[8] M. Vieira, S. Sergeenkov, and C. Furtado, Phys. Rev. A **96**, 013852 (2017).
[9] P. St-Jean, V. Goblot, E. Galopin, A. Lemaître, T. Ozawa, L. L. Gratiet, I. Sagnes, J. Bloch, and A. Amo, Nat. Photonics **11**, 651 (2017).
[10] S. Barik, A. Karasahin, C. Flower, T. Cai, H. Miyake, W. DeGottardi, M. Hafezi, and E. Waks, Science **359**, 666 (2018).
[11] W. Gao, B. Yang, B. Tremain, H. C. Liu, Q. H. Guo, L. B. Xia, A. P. Hibbins, and S. Zhang, Nat. Commun. **9**, 950 (2018).
[12] Z. Gao, F. Gao, Y. M. Zhang, Y. Luo, and B. L. Zhang, Adv. Opt. Mater. **6**, 1800532 (2018).
[13] O. Zilberberg, S. Huang, J. Guglielmon, M. Wang, K. P. Chen, Y. E. Kraus, and M. C. Rechtsman, Nature (London) **553**, 59 (2018).
[14] M. A. Bandres, S. Wittel, G. Hararl, M. Parto, J. Ren, M. Segev, D. N. Christodoulides, and M. Khajavikhan, Science **359**, eaar4005 (2018).
[15] J. Noh, W. A. Benalcazar, S. Huang, M. J. Collins, K. Chen, T. L. Hughes, and M. C. Rechtsman, Nat. Photonics **12**, 408 (2018).
[16] X. Zhu, H. X. Wang, C. Q. Xu, Y. Lai, J. H. Jiang, and S. John, Phys. Rev. B **97**, 085148 (2018).
[17] K. J. Fang, Z. F. Yu, and S. H. Fan, Nat. Photonics **6**, 782 (2012).
[18] M. Hafezi, E. A. Demler, M. D. Lukin, and J. M. Talor, Nat. Photonics **7**, 907 (2011).
[19] M. Hafezi, S. Mittal, J. Fan, A. Migdall, and J. M. Taylor, Nat. Photonics **7**, 1001 (2013).
[20] C. He, X. C. Sun, X. P. Liu, M. H. Lu, Y. L. Chen, L. Feng, and Y. F. Chen, Proc. Natl. Acad. Sci. USA **113**, 4924 (2016).
[21] W. Gao, M. Lawrence, B. Yang, F. Liu, F. Fang, B. Béri, J. Li, and S. Zhang, Phys. Rev. Lett. **114**, 037402 (2015).
[22] S. Y. Huo, J. J. Chen, H. B. Huang, and G. L. Huang, Sci. Rep. **7**, 10335 (2017).
[23] A. Slobozhanyuk, S. H. Mousavi, X. Ni, D. Smirnova, Y. S. Kivshar, and A. B. Khanikaev, Nat. Photonics **11**, 130 (2017).
[24] Y. T. Yang, Y. F. Xu, T. Xu, H. X. Wang, J. H. Jiang, X. Hu, and Z. H. Hang, Phys. Rev. Lett. **120**, 217401 (2018).
[25] R. Chaunsali, C. W. Chen, and J. Yang, Phys. Rev. B **97**, 054307 (2018).
[26] W. J. Chen, Z. Q. Zhang, J. W. Dong, and C. T. Chan, Nat. Commun. **6**, 8183 (2015).
[27] L. H. Wu and X. Hu, Phys. Rev. Lett. **114**, 223901 (2015).
[28] Y. Liu, Y. Ke, H. Lou, and S. Wen, Nanophotonics **6**, 51 (2017).
[29] L. Cai, M. X. Liu, S. Z. Chen, Y. C. Liu, W. X. Shu, H. L. Luo, and S. C. Wen, Phys. Rev. A **95**, 013809 (2017).
[30] W. J. M. Kort-Kamp, Phys. Rev. Lett. **119**, 147401 (2017).
[31] W.-M. Deng, X.-D. Chen, F.-L. Zhao, and J.-W. Dong, J. Opt. **20**, 014006 (2018).
[32] X. J. Piao, S. Yu, and N. Park, Phys. Rev. Lett. **120**, 203901 (2018).
[33] J. W. Dong, X. D. Chen, H. Y. Zhu, Y. Wang, and X. Zhang, Nat. Mater. **16**, 298 (2017).

[34] J. Noh, S. Huang, K. P. Chen, and M. C. Rechtsman, Phys. Rev. Lett. **120**, 063902 (2018).
[35] M. I. Shalaev, S. Desnavi, W. Walasik, and N. M. Litchinitser, New. J. Phys. **20**, 023040 (2018).
[36] F. Gao, H. R. Xue, Z. J. Yang, K. F. Lai, Y. Yu, X. Lin, Y. D. Chong, G. Shvets, and B. L. Zhang, Nat. Phys **14**, 140 (2017).
[37] X. Ni, D. Purtseladze, D. A. Smirnova, A. Slobozhanyuk, A. Alù, and A. B. Khanikaev, Sci. Adv. **4**, eaap8802 (2018).
[38] T. Dubček, C. J. Kennedy, L. Lu, W. Ketterle, M. Soljačić, and H. Buljan, Phys. Rev. Lett. **114**, 225301 (2015).
[39] L. Lu, Z. Y. Wang, D. X. Ye, L. X. Ran, L. Fu, J. D. Joannopoulos, and M. Soljačić, Science **349**, 622 (2015).
[40] L. Lu, L. Fu, J. D. Joannopoulos, and M. Soljačić, Nat. Photon. **7**, 294 (2013).
[41] Q. H. Yan, R. J. Liu, Z. B. Yan, B. Y. Liu, H. S. Chen, Z. Wang, and L. Lu, Nat. Phys. **14**, 461 (2018).
[42] Z. Wang, Y. Chong, J. D. Joannopoulos, and M. Soljačić, Nature (London) **461**, 772 (2009).
[43] X. Y. Ao, Z. F. Lin, and C. T. Chan, Phys. Rev. B **80**, 033105 (2009).
[44] J. Lu, L. F. Shen, X. H. Deng, X. E. Li, and X. D. Zheng, Appl. Opt. **52**, 5216 (2013).
[45] S. Y. Liu, W. L. Lu, Z. F. Lin, and S. T. Chui, Phys. Rev. B **84**, 045425 (2011).
[46] S. Y. Liu, W. L. Lu, Z. F. Lin, and S. T. Chui, Appl. Phys. Lett. **97**, 201113 (2010).
[47] S. A. Skirlo, L. Lu, and M. Soljačić, Phys. Rev. Lett. **113**, 113904 (2014).
[48] S. A. Skirlo, L. Lu, Y. Igarashi, Q. H. Yan, J. D. Joannopoulos, and M. Soljačić, Phys. Rev. Lett. **115**, 253901 (2015).
[49] Z. Wang, Y. D. Chong, J. D. Joannopoulos, and M. Soljačić, Phys. Rev. Lett. **100**, 013905 (2008).
[50] Y. Poo, R. X. Wu, Z. F. Lin, Y. Yang, and C. T. Chan, Phys. Rev. Lett. **106**, 093903 (2011).
[51] J. Lian, J. X. Fu, L. Gan, and Z. Y. Li, Phys. Rev. B **85**, 125108 (2012).
[52] Z. Li, R. X. Wu, Q. B. Li, Z. F. Li, P. Yin, R. J. Liu, and Z. Y. Li, Opt. Express. **23**, 9658 (2015).
[53] M. Kohmoto and Y. Hasegawa, Phys. Rev. B **76**, 205402 (2007).
[54] R. Bose, J. F. Mcmillan, J. Gao, and C. W. Wong, Appl. Phys. Lett. **95**, 131112 (2009).
[55] S. A. Schulz, J. Upham, L. O'Faolain, and R. W. Boyd, Opt. Lett. **42**, 3243 (2017).